Enhanced thermoelectric performance via the solid solution formation: The case of pseudobinary alloy $(Cu_2Te)(Ga_2Te_3)_3$ upon Sb substitution for Cu

Jiaolin Cui[1*], Xianglian Liu[1], Zhengliang Du[1],Yimin Chao[2*]

Abstract: In this work we have observed the beneficial effect from the solid solution formation on the thermoelectric performance of $(Cu_{2(1-x)}Sb_{2x}Te)(Ga_2Te_3)_3$ upon Sb substitution for Cu. This substitution allows the mixed occupations of Sb in the crystal lattice, i.e. Sb at Cu sites with $x\leq0.05$ and at Ga sides with $x\geq0.05$, which has resulted in the Pisarenko relation does not exactly capture the measured Seebeck coefficient under assumed effective masses m^*. The reduction of the lattice thermal conductivity (κ_L) has been quantified within the temperature range from room temperature to 723 K. Over the entire composition range, the κ_L value is reduced by 33% and 25% at temperature 723 K and 580 K, respectively. This observation is in a good agreement with the theoretical calculation based on the Callaway model used in the solid solutions. Along with the increasing of the mobility and electrical conductivity, the thermoelectric performance has been improved with the highest *ZT* value of 0.58 at 723 K, which is about double the value of intrinsic $(Cu_2Te)(Ga_2Te_3)_3$.

Keywords:

1. Introduction

Although the transformation of waste heat into useful electric power is very attractive so far, the conversion effectiveness is still low because of poor thermoelectric (TE) performance of the materials. Therefore, searching for new materials is one of the great challenges facing the members of TE research community. The TE performance is directly dependent on the dimensionless figure of merit (*ZT*),

$$ZT=T\alpha^2\sigma/\kappa \qquad (1)$$

where T, α, σ and κ are the absolute temperature, Seebeck coefficient, electrical conductivity, and total thermal conductivity with lattice contribution (κ_L) and electronic part (κ_e), respectively. The correlation among physical parameters above results in a very limited choice of the current state-of-the-art TE materials.

Among the currently developed state-of-the-art TE materials, a few binary chalcogenides, such as SnSe,[1,2] In_4Se_3[3-6] and PbTe,[7,8] have been explored extensively; while the ternary chalcogenides, such as $CuGaTe_2$[9-11] and $CuInTe_2$,[12-15] have also attracted research interests in recent years because of their unique crystal structures.

It was reported that Ga_2Te_3 forms pseudobinary alloys with Cu_2Te in a wide range of compositions $(Cu_2Te)_{1-y}(Ga_2Te_3)_y$. However, the total cations (Cu^++Ga^{3+}) in this compound is 2, less than anions Te^{2-} (2y+1) at $0.5\leq y<1.0$, hence (2y-1)/(2y+1) of cation sites are structural vacancies.[16] The structural vacancy is essential to the carrier concentration and lattice thermal conductivity. For example, at y=0.75, i.e. $(Cu_2Te)(Ga_2Te_3)_3$ (denominated as CTGT), one fifth of the cation sites are structural vacancies. The carrier concentration (n_H) in CTGT at room temperature (RT) reaches $0.53\sim1.2\times10^{25}$ m^{-3},[16,17] very close to the optimal n_H value ($10^{25}\sim10^{26}$ m^{-3})[18]. While at y=0.5, none of the cation sites are structural vacancies, the n_H value at RT is only 2.1×10^{24} m^{-3}.In addition, the κ value of the former ($\kappa\approx1.1$ $Wm^{-1}K^{-1}$) is lower than that of the latter ($\kappa\approx2.2$ $Wm^{-1}K^{-1}$) at 750 K.[19]Hence, the former should have a more prospective to be a potential TE candidate than the latter. However, the *ZT* value of CTGT is still low (ZT≈0.22 @ 735 K),[16] due to low electrical conductivity and relatively high thermal conductivity of lattice contribution ($\kappa_L\approx1.0$ $WK^{-1}m^{-1}$ @ 700K).[17] In order to reduce the κ_L, it is necessary to introduce extra point defects via the solid solution

formation..

The formation of solid solution has been long considered as an effective approach to better thermoelectric performance owing to the reduction of lattice thermal contribution caused by the phonon scattering from disordered atoms.[20] However, such a beneficial effect could often be neutralized by a reduction in mobility (μ) or carrier concentration (n_H) due to the alteration of chemical environment. In this regard, it is pivotal to select a proper dopant to stabilize the carrier concentration, while the mobility remains high simultaneously. Another big challenge is the solubility limit of dopants in many compounds, such as, Zn in $CuInTe_2$[21] and $AgInSe_2$,[22] which limits the beneficial effect to a certain extent.

Considering the atomic radius and solubility limit of foreign impurity in CTGT, it is believed that Sb might be one of the proper elements that has a relatively large solubility due to its smaller radius (1.53Å) than those of Ga (1.81Å) and Cu (1.57Å).[23] Upon its isoelectronic substitution for Ga^{3+}, it creates a defect Sb_{Ga} with no extra electron charges introduced; while the substitution for Cu^{+} generates Sb_{Cu}^{2+} acting as a donor. Although the creation of Sb_{Cu}^{2+} may reduce the *p*-type carrier concentration, it compensates the loss of the carrier mobility. In addition, the existence of mixed point defects (Sb_{Ga}, Sb_{Cu}^{2+}) could significantly decrease the total relaxation time (τ) of phonons, according to the Matthiessen's rule.[20] Therefore, a significant improvement of TE performance can be anticipated.

In this work, we substitute the element Sb for Cu in CTGT to introduce an extra copper vacancy, and then determine the exact Sb occupation sites through XPS and Raman spectra analyses. Through the solid solution formation upon Sb incorporation, both the electrical and thermal properties have been optimized, which leads to the remarkable improvement in TE performance.

2. Experimental

According to the chemical formula $(Cu_{2(1-x)}Sb_{2x}Te)(Ga_2Te_3)_3$, the four elements, Cu, Ga, Te and Sb with the purity of more than 99.999% were loaded into different vacuum silica tubes. Then, the mixtures were melted at 1273 K for 24 h, followed by slow cooling to 663 K, at which the ingots were annealed for 240 h. The detailed preparation procedures are similar to those reported in the previous publication.[21]

The Hall coefficients (R_H) were measured at room temperature (RT) and 390 K using a Physical Property Measurement System (PPMS, Model-9) with a magnetic field sweeping between ±2.0 T, and the Hall carrier concentration (n_H) and mobility (μ) were calculated according to the relations $\mu = R_H\sigma$ and $n_H = 1/(eR_H)$, respectively, where *e* is the electron charge.

The measurement of thermal diffusivities were conducted using a TC-1200RH at RT~723 K. The heat capacities (C_p) were estimated according to the relation $C_p = C_v + BT$ for the Cu–Ga–Te compounds, where the fitted *B* value is determined to be 0.015 J mol^{-1} K^{-2}.[24] Here the C_v values were estimated from the Dulong–Petit limit.

The other experimental details, such as the analyses of compositions (EPMA), XPS and Raman spectra, as well as the measurements of the physical parameters (α, σ, absorption coefficients *A*, etc.), have been reported in earlier publications.[21,25]

3. Results and discussion

3.1 X-ray diffraction patterns and chemical compositional analyses

Fig.S1 shows the x-ray diffraction patterns of powders $(Cu_{2(1-x)}Sb_{2x}Te)(Ga_2Te_3)_3$ with x=0~0.2, in which materials exhibit the pure phase of CTGT-based solid solution (PDF:058-0248) in the composition range x=0~0.1. At x=0.2, trace impurity phase Sb_2Te_3 (PDF:72-1990)is identified, indicating that the solubility of Sb in CGT is less than 0.2. Fig.1 presents the lattice parameters *a* and *c* values as a function of Sb content. At x=0 the *a* and *c* values (a=6.018 Å, c=11.902 Å) are larger than those from Plirdpring et al. (a=5.932 Å, c=11.825 Å).[16] It is interesting that both the *a* and *c* values show a decreasing tendency with Sb content

increasing in the range of $x \leq 0.05$, and then remain relatively constant. Such a non-linear relation seems that the element Sb is not completely incorporated into the CTGT crystal lattice. However, after XPS and Raman spectra analyses (see the discussion below), it is explainable that the non-linear relation is mainly attributed to the mixed occupation of Sb, allowing the disagreement with the Vegard's law.

The element distributions and chemical compositions for the sample at x=0.1 have been determined from EMPA mappings (Fig.S2a-d) and EDX spectrum (Fig.S2e and Table S1 in Supporting Information), where the Te molars are normalized to 5. Generally, the identified relative molars of Cu, Ga, Te and Sb are close to nominal ones, which suggest that the compositions in the final samples are almost as designed.

3.2 XPS and Raman spectra analyses

In order to analyze the oxidation states of the elements, the XPS core level spectra of four elements are recorded in Fig.S3(a-d), and the binding energy values (BE) at peak positions are listed in Table S2. The BE value of $Cu2p_{3/2}$ at x=0.1 is around 932.55 eV, almost identical to that for x=0 (~932.50 eV) (Fig.S3a), confirming the existence of Cu^{+}.[26] Similarly, the $Ga2p_{3/2}$ peak position from the sample with x=0.1 is at the same position as x=0 (Fig.S3b), i.e. the Ga^{3+} (1117.65~1117.75 eV) is identified.[27] Fig.S3c represents the XPS a spectrum of Sb3d, with a binding energy value of 530.52 eV for the $Sb3d_{5/2}$ and 539.8 eV for $Sb3d_{3/2}$. These point to a 3+ valence state for Sb.[28-30] In the core level Te3d spectrum (x=0.1), see Fig.S3d, the $Te3d_{3/2}$ and $Te3d_{5/2}$ doublet could be deconvoluted into 4 Gaussian peaks labeled $Te3d_{3/2}$ (1) (583.10 eV), $Te3d_{3/2}$ (2) (586.80 eV), $Te3d_{5/2}$ (3) (572.80 eV) and $Te3d_{5/2}$ (4) (576.15 eV).[31] The four Gaussian peaks in the Te3d spectra are corresponding to different bonding states of Te atoms,[32] and confirm the presence of Te^{2-}. Both $Te3d_{3/2}$ and $Te3d_{5/2}$ peaks upon Sb incorporation have a subtle shift towards the high binding energy side, which is attributed to the formation of Sb-Te bond. The shift in binding energy upon Sb-incorporation suggests that Te has donated electrons to Sb because the binding energies corresponding to $3d_{5/2}$ and $3d_{3/2}$ transitions have been increased.[32]

Since the Sb^{3+} has an ionic radius of 0.76 Å and electronegativity =2.05, it is expected to occupy the Cu sites (ionic radius of Cu^{+} = 0.77 Å, electronegativity =1.9), which is leading to the overlap of wave function of antimony with tellurium for the formation of the Sb-Te bond.[31] The occupation of Sb in Cu sites below $x \leq 0.05$ can also be verified by the shrinkage of crystal lattice, as shown in Fig.1.

In order to determine the exact occupation sites of Sb, the Raman spectra of four samples (x=0, 0.05, 0.1 and 0.2) are analyzed, shown in Fig.2a. The results show that the Raman spectra of Sb-incorporated samples possess the resemblance to that of intrinsic CTGT, which suggests that the molecular structures are rather similar and remain long-range ordered. However, if one takes a close look at the spectra, it is found that upon a limited Sb incorporation ($x \leq 0.05$) there is a shift of the main mode at 133 cm^{-1} towards the high energy side (blue shift), as shown in the magnified plot Fig.2b. Fig.2c is the relation between the wavenumbers of the main mode (133 cm^{-1}) and x value, where the wavenumbers increase with x value increasing. However, with x>0.05, there is no further blue shift observed. Usually, Raman shift is indicative of internal stress/strain of the materials. The blue shift upon Sb incorporation ($x \leq 0.05$) suggests the presence of the compressive stress, which is likely caused by the occupation of Sb into the Cu sites. At x>0.05 the extra Sb atoms would occupy the Ga sites (ionic radius of Ga^{3+}=0.62 Å) due to the saturation of Sb in Cu sites, which creates the tensile stress neutralizing the compressive stress generated by Sb occupation at Cu sites. That is the reason why there is no further Raman shift at x>0.05. Owing to the mixed occupations of Sb which creates opposite stresses, the nonlinear dependences of the lattice parameters a and c on Sb content are thus observed, see Fig. 1.

3.3 Transport properties and TE performance

The presence of mixed occupations of Sb might alter the chemical environment of CTGT. In order to

identify the beneficial effect on the transport properties, we have measured the Hall coefficient at RT and 390 K. The calculated Hall carrier concentration (n_H) and mobility (μ) are displayed in Fig.3, where the n_H value from Plirdpring at RT for the CTGT is presented for comparison. [16] The n_H values at x=0, which are n_H = 2.29 ×10^{25} m^{-3} at RT and n_H = 2.48 ×10^{25} m^{-3} at 390 K respectively, decrease to 3.31×10^{24} m^{-3} and 1.53×10^{25} m^{-3} at x=0.05. At x≥0.05 the n_H value remains relatively stable (2.55~5.50 ×10^{24} m^{-3} at RT and 1.13~1.53 ×10^{25} m^{-3} at 390 K). At RT the mobility increases with Sb content increasing until x=0.1, and then decreases; while the μ value at 390 K shows an increasing tendency over the entire Sb content range.

The TE properties as a function of temperature are presented in Fig.4. The Seebeck coefficient (α) values are positive for all samples, indicating the p-type semiconducting behavior. Generally, the α value increases with the temperature increasing, and then decreases from the maximum value due to intrinsic excitation of carriers. In addition, the α value decreases with Sb content increasing in the low temperature region. The peak α value gradually decreases from 272.57 μV.K^{-1} at 541 K (x=0) to 231.38 μV.K^{-1} at 612 K (x=0.2) as Sb content increases (Fig.4a).

Unlike the composition dependence of α value, the electrical conductivity (σ) increases with the temperature increasing for all the samples. The sample at x=0.05 gives the highest σ value (8.8×10^3 $\Omega^{-1}m^{-1}$) at 723 K (Fig.4b), which is mainly due to the gradual increasing of the mobility μ.

The lattice thermal conductivity (κ_L) against temperature is plotted in Fig.4c, where some points in the curves are intercalated for clarity. Generally, the lattice part (κ_L) reduces with temperature increasing, except for the high Sb content samples (x=0.1 and 0.2), which reveal a bipolar effect, as shown in Fig4c. However, if we do a 1/T fitting from low temperatures to estimate the lattice parts (κ_L), a reduction of κ_L with Sb content increasing can be seen, despite that the sample at x=0.02 gives relatively low κ_L values at high temperatures. The inset in Fig4c is total thermal conductivity (κ), which behaves similarly to the lattice contributions κ_L, suggesting that the heat carrying by phonons is dominant in the materials.

Fig.4d is the dimensionless figure of merit (ZT), and the results from Ye[17] are presented for comparison. It is observed that the sample at x=0.05 gives the highest ZT value (0.58 at 723 K), which is about two times that of the intrinsic CTGT, and 0.35 higher than the reported value 0.23.[16] This result indicates that the solid solution formation via the mixed Sb occupations is an effective approach to optimize the TE performance.

The abnormal variation of the Hall carrier concentration with Sb content might be related to the structural modification. In order to have a better understanding on the alteration of the band structure, the Pisarenko relations are presented in Fig.5, assuming the hole effective mass m* equal to m*= 0.14, 0.19, 0.29 and 0.83m_e at RT (Fig.5a), and m* = 0.42, 0.64, and 0.98m_e at 390 K (Fig.5b), respectively. The data labeled by ★ represent measured α values in this work. It is observed that the Pisarenko relations do not exactly capture the measured values of Seebeck coefficient under assumed effective masses m*, and the α values at RT and 390 K rather increase with the carrier concentration increasing. This implies that the electronic band structure suffers some alteration upon mixed Sb occupations in CTGT.[33,34] However, the bandgap (E_g) seems not change, because the measured E_g value remains almost unchanged (E_g=0.85~0.90 eV) with Sb content increasing (See Fig.S4). In fact, if one takes a close look at the Seebeck coefficients shown in Fig.4a, one can find that the peak α value for each sample generally decreases, while the peak temperature (T_{max}) at which the highest α value (α_{max}) appears gradually increases (see the arrow in the Fig.4a). This suggests that the bandgap E_g, according to the estimation E_g =2|α_{max}|eT_{max},[35] is kept constant, although the recent investigation reveals that a deviation of more than one factor of two occurs 35.[36] Therefore, the band structure alteration is likely attributed to the energy gap (ΔE_A) between impurity level (E_i) and valence band (E_{VBM}), i.e. ΔE_A=E_i-E_{VBM}, which might increase at x≤0.5, and remain stable at x≥0.5 at high temperatures,[33,37] based on the first approximation:

$$n_p(T) \approx A(T)\exp(-\frac{\Delta E_A}{\kappa_B T}) \quad (2)$$

The increasing of ΔE_A at $x \leq 0.5$ can be ascribed to the creation of defect Sb_{Cu}^{2+} acting as a donor, thus causing the electron-hole compensation; while the stable value of ΔE_A at $x \geq 0.5$ is due to the fact that there is no net charge generated via the isoelectronic substitution of Sb for Ga, which allows the Hall carrier concentration to remain constant. Therefore, x=0.05 is the critical Sb content at which the sample possesses the highest electrical conductivity.

Moreover, the mobility (μ) exhibits increasing tendency with Sb content increasing at 390 K, which conflicts with the many observations. For example, Wang [20] and Bux et al.[38] observed that in the solid solutions $(PbTe)_{1-x}(PbSe)_x$ and $Mg_2Si_{1-x}Bi_x$ the mobility generally decreases with the impurity content increasing due to the reduction of total relaxation time. The abnormal behavior of the mobility in the present materials might be also ascribed to the abnormal variation in energy gap (ΔE_A) with Sb content increasing, which results in the Seebeck coefficient vs. carrier concentration is not in the exact single parabolic band (SPB) relation.

Through the estimation of the lattice part (κ_L) using $1/T$ fitting from the low temperature, we observed that the lattice contributions (κ_L) generally reduce with Sb content increasing at high temperatures. The reduction of κ_L with Sb content increasing is anticipated due to the increased phonon scattering caused by the formation of solid solution. , As shown in Fig.6, three sets of κ_L values (at RT, 580 K and 723 K) exhibit similar behaviour as Sb content increasing. However, the κ_L value at 723 K is about 33% lower than that at RT, that is, $\frac{\kappa_{L,723K}}{\kappa_{L,RT}} \approx \frac{2}{3} = 0.67$, while at 580 K it is 25% lower, i.e., $\frac{\kappa_{L,580K}}{\kappa_{L,RT}} \approx \frac{3}{4} = 0.75$.

To confirm the above reduction in κ_L as temperature increases, we estimate the variation tendency of the κ_L value based on the model proposed by Callaway et al.[39] Because the κ_L value in solid solutions is roughly proportional to $(T)^{-1/2}$ at a given composition at high temperatures,[39] that is,

$$\kappa_L = \frac{K}{4\pi v_s (A\,C\,T)^{\frac{1}{2}}} \quad (3)$$

where A is a composition related parameter, and is defined by:

$$A = \frac{\Omega}{4\pi v_s^3} c(1-c)(\frac{\Delta M}{M})^2 \quad (4)$$

K is the Boltzmann's constant, C is a constant, v_s is the velocity of sound (2.28×10^3 m/s),[40,41] which is assumed not varying with composition, Ω is the volume of the unit cell, and c is the relative concentration of pure material (c>0.5 in the present solid solutions).

If we neglect the little difference of the values $[c(1-c)\Omega(\frac{\Delta M}{M})^2]^{-\frac{1}{2}}$ among different samples in Eq.4, the $\frac{\kappa_{L,723K}}{\kappa_{L,RT}}$ and $\frac{\kappa_{L,580K}}{\kappa_{L,RT}}$ values can be estimated based on the Eq.3, that is, $\frac{\kappa_{L,723K}}{\kappa_{L,RT}} = \left(\frac{T_{RT}}{T_{723K}}\right)^{\frac{1}{2}} = \left(\frac{298}{723}\right)^{\frac{1}{2}} = 0.64$ and $\frac{\kappa_{L,580K}}{\kappa_{L,RT}} = \left(\frac{T_{RT}}{T_{580K}}\right)^{\frac{1}{2}} = \left(\frac{298}{580}\right)^{\frac{1}{2}} = 0.72$. These values are in good agreement with the experimental data 0.67 and 0.75.

On the other hand, if the values $[c(1-c)\Omega(\frac{\Delta M}{M})^2]^{-\frac{1}{2}}$ in Eq.4 among different samples should be taken

into consideration, the κ_L value is directly proportional to the product $[c(1-c)\Omega(\frac{\Delta M}{M})^2]^{-\frac{1}{2}}(T)^{-\frac{1}{2}}$ (c>0.5, 0<x≤0.5 assuming the solid solution in this composition range), where the parameters of c, Ω and $\Delta M/M$ are calculated in Table 1. After plotting the relation between the $[c(1-c)\Omega(\frac{\Delta M}{M})^2]^{-\frac{1}{2}}(T)^{-\frac{1}{2}}$ product against x value, we have observed that the values $[c(1-c)\Omega(\frac{\Delta M}{M})^2]^{-\frac{1}{2}}(T)^{-\frac{1}{2}}$ at RT, 580 K and 723 K gradually decrease with the x value increasing, as shown in Fig.6b. The higher the temperature, the lower the $[c(1-c)\Omega(\frac{\Delta M}{M})^2]^{-\frac{1}{2}}(T)^{-\frac{1}{2}}$ value. Therefore, the κ_L values decrease with both the temperature and x value increasing in due course. It is worth noting that the estimated tendencies of κ_L for a given constant C in Eq.3 are in agreement with the experimental data roughly (see Fig.6a in dotted lines), which confirms that the Callaway model works well in the phonon scattering process, assuming that the existing phonon scattering mechanism consists of the Umklapp scattering and point defect scattering mainly, and that only the following factors are considered: the mass difference, binding force difference and strain field induced by the point defect in the present solid solutions.[20,39, 42,43]

4. Conclusions

In this work the solid solutions $(Cu_{2(1-x)}Sb_{2x}Te)_{0.5}(Ga_2Te_3)_{1.5}$ (x=0~0.2) have been synthesized and their thermoelectric properties have been examined. The analyses from XPS and Raman spectra have proved that the element Sb prefers to the Cu site when x≤0.05, which reduces the Hall carrier concentration (n_H) as Sb content increases. However, after the extra Sb atoms occupy the Ga sites at x≥0.05, the n_H values remain relatively stable. The mobility (μ) measurement shows a different composition dependence. It is worth noting that the κ_L values measured at 723 K and 580 K have dropped by 33% and 25%, respectively, in comparison with those at RT. These observations are in a good agreement with the estimations based on the model proposed by Callaway et al. used in solid solutions. Owing to the beneficial effect of the solid solution formation upon Sb incorporation, the thermoelectric performance is significantly improved with a ZT value of 0.58 at 723 K.

Acknowledgements

This work is supported by the National Natural Science Foundation of China (51671109, 51171084), Zhejiang Provincial Natural Science Foundation (LY14E010003). We are grateful to the contribution to the analyses of the experimental results by Wei Ren and Professor Shaoping Chen from Taiyuan University of Technology.

Notes and references

[1] School of Materials & Chemical Engineering, Ningbo University of Technology, Ningbo 315016, China.

[2] School of Chemistry, University of East Anglia, Norwich NR4 7TJ, United Kingdom

* Corresponding authors, J. L. Cui, E-mail: cuijiaolin@163.com; Y. Chao, E-mail:Y.Chao@uea.ac.uk

Electronic Supplementary Information (ESI) available: XRD patterns, EPMA mapping, chemical composition, XPS spectra and binding energy (BE) values, and the absorption coefficients analyses, See DOI: 10.1039/b000000x/

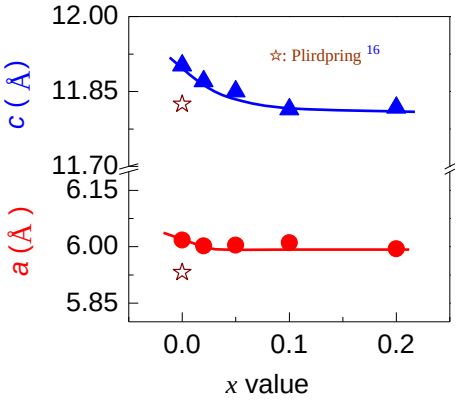

Fig.1 The lattice parameters *a* and *c* values as a function of *x* value. The data from Plirdpring et al.[16] are presented for comparison.

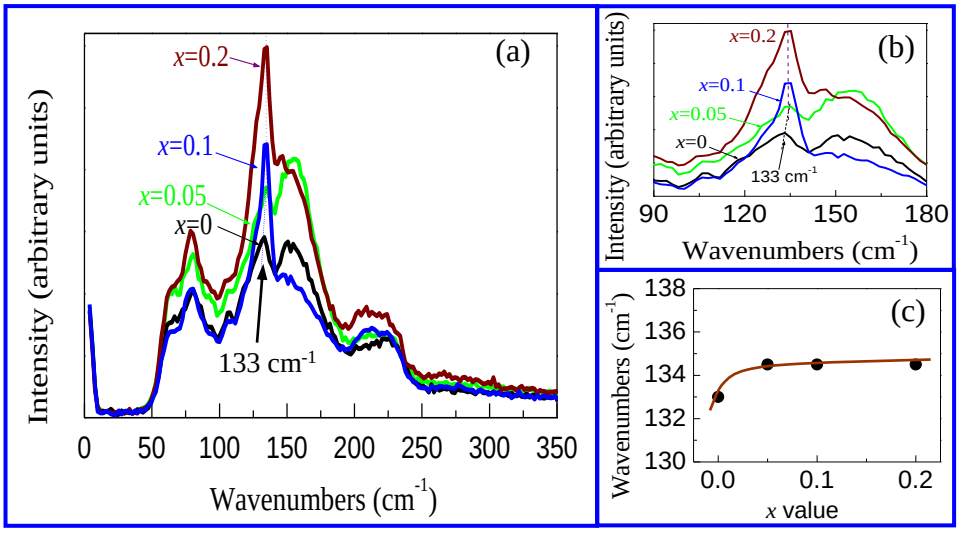

Fig.2 The Raman spectra of four samples (*x*=0, 0.05, 0.1 and 0.2). (a) Full Raman spectra; (b) Close-up view of the spectra; (c) The wavenumbers of the main mode (133 cm^{-1}) as a function of *x* value.

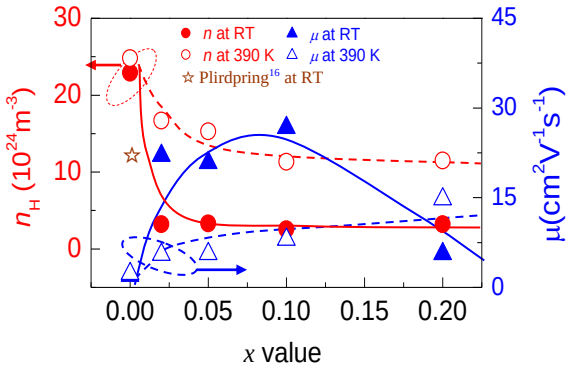

Fig.3 The Hall carrier concentrations (n_H) and mobility (μ) at RT and 390 K as a function of *x* value. The data from Plirdpring et al.[16] are presented for comparison.

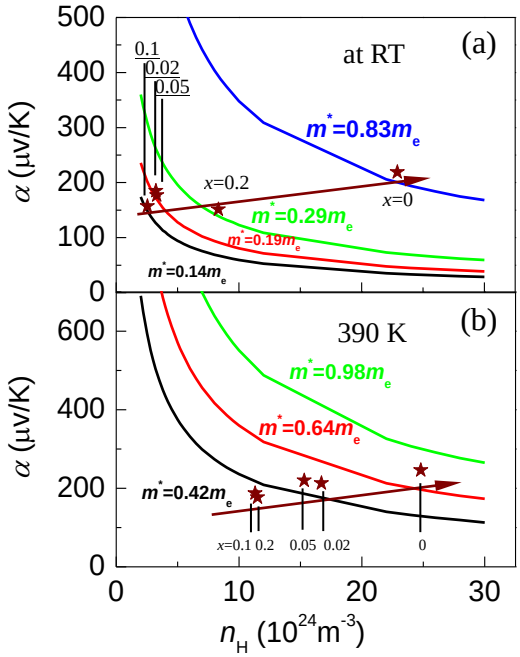

Fig. 5. The Pisarenko plots assuming: (a) m^* =0.83, 0.29, 0.19m_e and 0.14 m_e at RT; (b) m^* =0.98, 0.64, and 0.42 m_e at 390 K. The data labeled by ★ represent the α values with determined n_H values in this work.

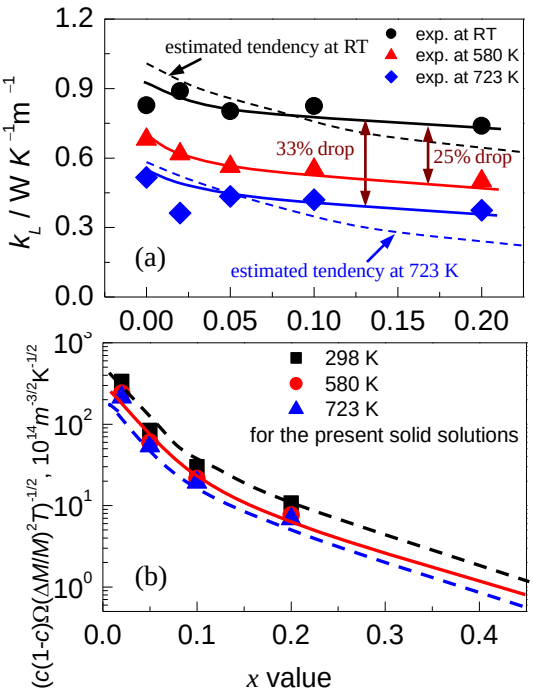

Fig. 6. (a) The lattice contributions (κ_L): at RT, 580 K and 723 K, as a function of x value. The dotted lines represent the κ_L values at RT and 723 K, estimated using Callaway et al.[39] model in solid solutions; (b) The estimated relation between the products $(c(1-c)\Omega(\Delta M/M)^2T)^{-1/2}$ and x value (c>0.5, 0<x≤0.5 assuming the solid solution in this composition range). The data labeled ■,●,▲ represent the present solid solutions.

Table 1 Some parameters of different compounds $(Cu_{2(1-x)}Sb_{2x}Te)(Ga_2Te_3)_3$

	Ω, 10^{28} (m^3)	c	ΔM / M	$c(1-c)\Omega(\Delta M/M)^2$, 10^{-34} (m^3)
x=0	8.6208	1.0	0	-----
x=0.02	8.5524	0.9978	0.0013	302.80
x=0.05	8.5428	0.9944	0.0032	48.11
x=0.1	8.5356	0.9890	0.0063	3.75
x=0.2	8.4932	0.9780	0.0127	0.29

References

1 L. Zhao, G.Tan, S.Hao, J.He, Y.Pei, H.Chi, H.Wang, S.Gong, H.Xu, V.P.Dravid, C.Uher, G.J.Snyder, C.Wolverton and M.G.Kanatzidis, ***Science***, 2016,**351**,141.

2 L. Zhao, S.Lo, Y.Zhang, H.Sun, G.Tan, C.Uher, C.Wolverton, V.P.Dravid and M.G.Kanatzidis1, ***Nature***, 2014,**508**, 373.

3 J.S. Rhyee, K.H. Lee, S.M. Lee, E.Cho, S. II Kim, E.Lee, Y.S.Kwon, J.H.Shim and G.Kotliar, ***Nature***, 2009,**459**, 965.

4 Z. Lin, L.Chen, L.Wang, J. Zhao and L.Wu, ***Adv. Mater.***, 2013, **25**, 4800.

5 J.Rhyee, K.Ahn, K.Lee, H.Ji and J.Shim, ***Adv. Mater***., 2011, **23**, 2191.

6 G. Han , Z.Chen , J. Drennan and J. Zou, ***Small***, 2014,**10**, 2747.

7 Y.Pei, X.Shi, A.LaLonde, H.Wang, L.Chen and G.J.Snyder, ***Nature***, 2011,**473**,66.

8 J.P.Heremans,V.Jovovic, E.S.Toberer, A. Saramat, K. Kurosaki, A.Charoenphakdee, S. Yamanaka, G.J. Snyder, Enhancement of thermoelectric efficiency in PbTe by distortion of the electronic density of states, ***Science*** 321, 2008, 554.

9 T.Plirdpring, K.Kurosaki, A. Kosuga, T.Day, S. Firdosy, V.Ravi, G.J.Snyder, A. Harnwunggmoung, T.Sugahara, Y.Ohishi, H.MuTa, S.Yamanaka, Chalcopyrite $CuGaTe_2$: A high□efficiency bulk thermoelectric material, ***Adv. Mater.***, 24, 2012, 3622.

10 J.Zhang, R.Liu, N.Cheng, Y.Zhang, J.Yang, C.Uher, X.Shi, L.Chen, W.Zhang, High-Performance Pseudocubic Thermoelectric Materials from Non-cubic Chalcopyrite Compounds, ***Adv. Mater.*** 26,2014, 3848.

11 X.Shi, L.Chen, C.Uher, Recent advances in high-performance bulk thermoelectric materials, Inter. Mater. Rev. **2016**, DOI: 10.1080/09506608.2016.1183075.

12 R.Liu, L.Xi, H.Liu, X.Shi, W.Zhang and L.Chen, ***Chem. Commun.***, 2012, **48**, 3818–3820.

13 N. Cheng, R.Liu, S.Bai, X.Shi, and L. Chen, ***J. Appl.Phys***. 2014,**115**, 163705.

14 J.Wei, H.J.Liu, L. Cheng, J. Zhang, J. H. Liang, P. H. Jiang, D. D. Fan, J. Shi, ***AIP Adv***. 2015,**5**,107230.

15 A.Kosuga, K.Umekage, M.Matsuzawa, Y.Sakamoto, I.Yamada, ***Inorg. Chem***. 2014, 53, 6844−6849.

16 T.Plirdpring, K.Kurosaki, A.Kosuga, M. Ishimaru, A.Harnwunggmoung, T.Sugahara, Y.Ohishi, H.Muta and S.Yamanaka, ***Mater. Trans***., 53, 2012,1212.

17 Z.Ye, J.Cho, M.M.Tessema, J.R.Salvador, R.A.Waldo, H.Wang, W.Cai, ***J.Solid State Chem.***, 201,2013, 262–269.

18 G. J. Snyder and E. S. Toberer, ***Nat. Mater.***, 2008, 7, 105.

19 K.Kurosak, S.Yamanaka, ***Phys. Status Solidi A***, 210,2013, 82–88.

20 H.Wang, Aaron D. LaLonde , Yanzhong Pei, and G. Jeffery Snyder, ***Adv. Funct. Mater.*** 2013, 23, 1586–1596.

21 J.Yang, S.Chen, Z.Du, X.Liu, J.Cui, ***Dalton Trans***. 2014, 43, 15228-15236.

22 L. Wang, P.Ying, Y.Deng, H.Zhou, Z.Du and J.Cui, ***RSC Adv***., 2014, 4, 33897.

23 M. L. Li, ***in Concise Handbook of Chemical Data***, Chemical Engineering Press, Beijing, 2003, p. 9, in Chinese.

24 D.F.Zou, S.H.Xie, Y.Y.Liu, J. Lin and J. Li, ***J. Alloys Compd***., 2013, 570, 150.

25 J. Cui, L.Wang, Z. Du, P. Ying and Y. Deng, ***J. Mater. Chem. C***, 2015, 3, 9069.

26 J. Yao, N. J. Takas, M. L. Schliefert, D. S. Paprocki, P. E. R.Blanchard, H. Gou, A. Mar, C. L. Exstrom, S. A. Darveau, P. F. P. Poudeu, and J. A. Aitken, ***Phys. Rev. B***, 84, 075203(2011).

27 J. F. Moulder and J. Chastain, ***Handbook of X-ray Photoelectron Spectroscopy: A Reference Book of Standard Spectra for Identification and Interpretation of XPS Data***, Perkin‐Elmer Corporation, Physical Electronics Division, Eden Prairie, Minnesota, 1992, p. 261.

28 K.B.Garg, P.Nordblad, M.Heinonen, N.Panwar, V.Sen, F.Bondino, E.Magnano, E.Carleschi, F.Parmigiani, S.K.Agarwal, ***J. Magnetism Magnetic Mater.***,2009, 321,305–311.

29 H. Bryngelsson, J.Eskhult, L.Nyholm, M.Herranen, O.Alm and K.Edström, ***Chem. Mater***. **2007,** *19*, 1170-1180.

30 Omar E. Linarez Pérez, Miguel D. Sánchez, Manuel López Teijelo, ***J.Electroanal.Chem.***, 2010, 645,143–148.

31 B.V.R. Chowdari, P. Pramoda Kumari, ***J. Non-Cryst. Solids***, 1996, 197, 31-40;

32 T. Potlog, D.Duca, M.Dobromir, ***Appl. Surf. Sci***., 2015, 352, 33–37.

33 J.Cui, Z.Sun, Z.Du and Y.Chao, ***J. Mater.Chem. C***, 2016, 4, 8014-8019.

34 Y.F.Liu, P.Sahoo, J.P.A.Makongo, X.Zhou, S.Kim, H.Chi, C.Uher, X.Pan, P.F.P.Poudeu, ***J.Am.Chem. Soc.***, 2013, **135**, 7486.

35 H. J. Goldsmid and J.W.Sharp, ***J. Elect. Mater.*** 1999, 28, 869–872.

36 Z.M.Gibbs, H.S. Kim, H.Wang, and G.J.Snyder, ***Appl. Phys.Lett***., 2015, 106, 022112.

37 C. Rincón, S. M. Wasim and G. Marín, ***Appl. Phys. Lett.***, 2002,80, 998.

38 S.K.Bux, M.T.Yeung, E.S.Toberer, G.J.Snyder, R.B.Kaner and J.P.Fleurial, ***J. Mater. Chem.***, 2011, 21, 12259

39 J. Callaway, H.C.von Baeyer, ***Phys Rev***. 1960, 120,1149.

40 A. Rivero, M. Quintero, C.H. Poer, J. Gonzalez, R. Tovar, J. Ruiz, ***J. Elect. Mater***. 1997, 26, 1428.

41 K. Bohmhammel, P. Deus, G, Kühn, W. Möller, ***Phys. Stat. Sol. A***, 1982, 71, 505.

42 R. Berman , ***Thermal Conduction in Solids***, Oxford University Press , Oxford 1976.

43 E. S. Toberer , A. Zevalkink , G. J. Snyder , ***J. Mater. Chem.*** 2011, 21, 15843.